SOIL CONSTITUTIVE MODEL FOR SUSTAINABLE GEOTECHNICAL DESIGN

William Higgins[1], Harry Martindale[1], Tanusree Chakraborty[2*] and Dipanjan Basu[1]

[1]Department of Civil and Environmental Engineering, University of Connecticut, Storrs, CT 06269, USA.
[*]Telephone 860 486 5023, E-mail: dbasu@engr.uconn.edu

[2]Department of Civil Engineering, Indian Institute of Technology Delhi, India.
*Telephone: +1 765 337 6019, *E-mail: tanusree.research@gmail.com

ABSTRACT: Design of sustainable civil infrastructure requires that the built environment is resilient against natural and man-made hazards which can cause catastrophic failures. As a result, high rates of strain (10^2-10^4/sec) are generated in the soil which plays a significant effect on the strength and stiffness of soil. In this paper, we investigate the high strain-rate behavior of sand by developing a rate-dependent, multi-axial, viscoplastic two-surface constitutive model based on the concepts of critical-state soil mechanics. Perzyna's overstress theory and non-associated flow rule are used in this model. The rate-dependent model parameters are determined from experimental data of split Hopkinson pressure bar test under high rate loading. Model performance is demonstrated for various sands.

1. INTRODUCTION

An important requirement of sustainable infrastructure design is that the built environment is resilient against natural and man-made disasters. Natural hazards like landslide, mudflow, debris flow, earthquake and tsunami and man-made hazards like terror attack and collision cause catastrophic failures in civil infrastructure. Hazardous flows (landslide, mudflow and debris flow) can move rapidly along down slope with a flow speed as high as 0.03 km/sec. Earthquake induced P and S wave speed can be up to 6 km/sec (Kumar et al. 1987, Tseng and Chen 2006). A bomb blast can create strain rates in materials up to 10^4/sec (DeSilva 2005, Barsoum and Philip 2007, Ishihara 1996). Often, large geo-structures like earth embankments, slopes and tunnels involving large masses of soil are affected by these hazards. As a result, high rates of strain, of the order of 10^2-10^4/sec, are generated in the soil. Soil is the weakest of all civil engineering materials and often collapse of a civil engineering structure is initiated from within the soil. In order to safeguard civil engineering facilities against different catastrophic hazards, it is essential that soils subjected to high strain rates are properly characterized and modeled. The rate of induced strain (or stress) plays a significant effect on the strength and stiffness of soil.

Casagrande and Shannon (1948) were the first to study the effect of strain rate on the strength of soil. They performed drained triaxial compression tests on dense Manchester sand with the strain rates varying from 1×10^{-5}/sec to 1/sec and observed that the compressive strength of sand increased by about 10% from the corresponding rate-independent (static) value. Since then, many researchers have performed drained and undrained triaxial tests on sand under different loading rates (Whitman and Healy 1962, Yamamuro and Lade 1998, Yamamuro and Abrantes 2003). Jackson et al. (1980) conducted uniaxial strain tests on sand at 200/sec strain rate. From these triaxial and uniaxial tests it was observed that the shear strength of sand increased by about 10% with each log-cycle increase in the strain rate and that an increase in the applied strain rate resulted in increased dilatancy and earlier peak generation. It was further observed that the dynamic shear modulus of sand was 5-40% higher than the static shear modulus. The split Hopkinson pressure bar (SHPB) tests have been performed on sand by several researchers in order to investigate sand behavior at strain rates as high as 10^4/sec (Felice 1985, Veyera and Ross 1995, Semblat et al. 1999, Song et al. 2009). The results showed that the compressive response of the dry sand was significantly dependent on the initial density, compaction and lateral confinement level. The stress-strain response of highly saturated sand (saturation > 80%) followed nearly the same slope as of the uniaxial stress-strain response of water under SHPB test.

Very few researchers (Laine and Sandvik 2001, Wang et al. 2004, Grujicic et al. 2006, Tong and Tuan 2007, Deshpande et al. 2009, Chakraborty et al. 2010) have attempted to develop soil

constitutive models for high strain rates. Although some of the existing constitutive models can capture strain rates as high as 200/sec and have been applied to simulate blast loading in soil, they are mostly not capable of capturing the path dependent, multi-axial soil behavior with all the important features like the peak and critical states and phase transformation under both rate-independent and rate-dependent loading.

In this paper, a rate-dependent, viscoplastic constitutive model for sand is developed that can simulate all the important features — e.g., dilatancy, critical state and phase transformation — of the multi-axial, stress-path dependent behavior of soil under both drained and undrained loading, and can capture extremely high strain rates. The model is developed by extending the modified Manzari-Dafalias two-surface plasticity model for sands (Manzari and Dafalias 1997, Papadimitriou and Bouckovalas 2001, Dafalias and Manzari 2004, Loukidis and Salgado 2009). Viscoplasticity is incorporated in the model using Perzyna's overstress theory (Perzyna 1963 and 1966). The strain-rate dependence of the initial shear modulus is incorporated explicitly in the model. The model performance is demonstrated by comparing with test results obtained from high-speed SHPB tests for up to 2000/sec strain rate. The research presented here is at the initial stages of an ongoing project on systematic quantification of soil behavior under high strain rates.

2. BASIC PLASTICITY MODEL

The rate-independent, two-surface sand plasticity model adopted in the study was proposed by Manzari and Dafalias (1997) and later modified by Loukidis and Salgado (2009). Figure 1(a) shows the model in the normalized deviatoric stress space. The model contains four conical shear surfaces, the yield, bounding, dilatancy and critical-state (CS) surfaces, with straight surface meridians and apex at the origin. The projection and interpolation rules are exclusively contained in the deviatoric plane. The yield surface of the model is given by

$$f = \sqrt{\rho_{ij}\rho_{ij}} - \sqrt{2/3}\, m = 0 \tag{1}$$

where m is the radius of the yield surface and ρ_{ij} is the stress ratio given by

$$\rho_{ij} = r_{ij} - \alpha_{ij} \tag{2}$$

in which r_{ij} is the normalized deviatoric stress tensor ($r_{ij} = s_{ij}/p'$; s_{ij} is the deviatoric stress tensor and p' is the effective mean stress) and α_{ij} is a kinematic hardening tensor.
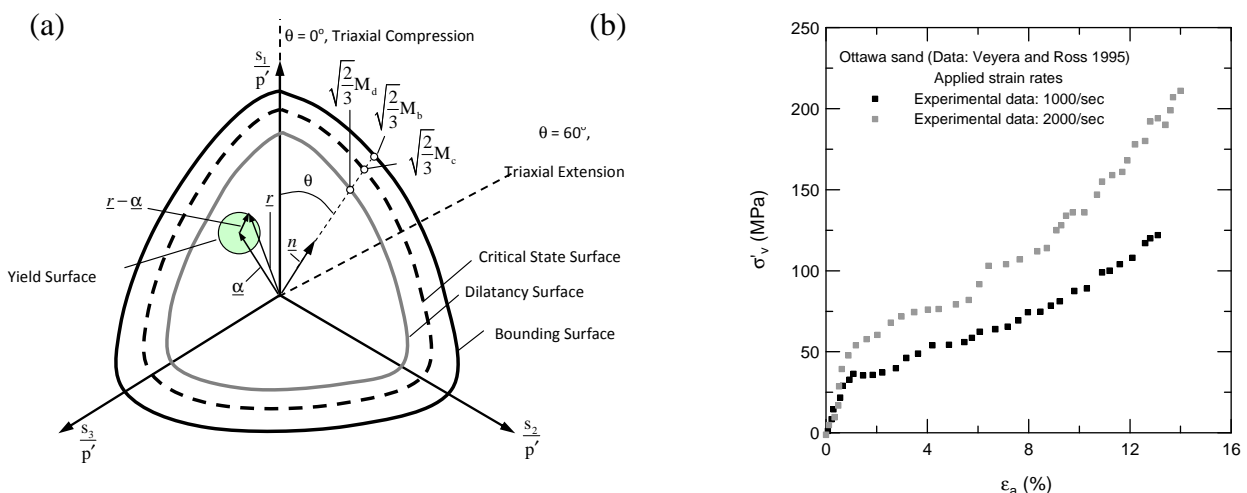
Figure 1. (a) Modified Manzari-Dafalias two-surface plasticity model for sand (from Loukidis and Salgado 2009) and (b) a typical vertical stress-axial strain plot for Ottawa sand in SHPB test (from Veyera and Ross 1995)

The yield surface can harden only kinematically through the use of the kinematic hardening tensor α_{ij}. The bounding and the dilatancy surfaces can harden or soften isotropically through the dependence of the corresponding stress ratios M_b and M_d on the state parameter ψ ($\psi = e - e_c$; where e

and e_c are the current and the critical-state void ratios at the same mean stress) (Been and Jefferies 1985)

$$M_b = g(\theta)M_{cc}e^{-k_b\psi} \tag{3}$$

$$M_d = g(\theta)M_{cc}e^{k_d\psi} \tag{4}$$

where M_{cc} is the critical-state stress ratio in triaxial compression [$M_{cc} = 3(\sigma'_{1,CS} - \sigma'_3)/(\sigma'_{1,CS} + 2\sigma'_3)$]. In the current model formulation, M_{cc} is a model parameter, k_b and k_d are fitting parameters and $g(\theta)$ is a function of the Lode's angle θ that determines the shapes of the critical-state, bounding and dilatancy surfaces on the deviatoric plane (Loukidis and Salgado 2009).

3. DEVELOPMENT OF THE HIGH STRAIN-RATE CONSTITUTIVE MODEL

Figure 1(b) illustrates a typical vertical stress vs. axial strain response of Ottawa sand under SHPB test under maximum strain rates of 1000/sec and 2000/sec at 0% saturation (data from Veyera and Ross 1995). Three important features of sand stress–strain behavior in impact loading are observed in this figure which the constitutive model needs to be able to capture: (1) an inertial response early in the event when the soil sample at rest is suddenly accelerated after initial contact with the striker bar; inertial response becomes more prominent at higher impact velocities (e.g., higher strain rates), (2) gradual transition from stiff initial inertial response to a viscous flow behavior and (3) a strain hardening behavior at large strains where the stress-strain response looks like an exponential curve. In the following sections we will discuss how the model captures the first two features. The third feature is captured through the evolution of α_{ij} (the kinematic hardening tensor).

3.1 Initial shear modulus

In the current model, the stress state is assumed nonlinear elastic inside the yield surface. The SHPB tests on sand (Veyera and Ross 1995, Semblat et al. 1999) showed that the initial shear modulus up to 1% of axial strain was between 300 to 6000 MPa, which is almost 5-40% higher than the shear modulus of sand in static loading. This increase in shear modulus is due to the inertial response of sand under suddenly applied impact load (as observed by Dupaix and Boyce 2007 for polymers). However, systematic quantification of the increase in shear modulus for sands is not yet done in the literature. Hence, in the current model, we use an curve-fitting approach through the experimental data for the very initial portion of the stress-strain response (i.e. when the axial strain is less than 1%). The initial shear modulus G_0 is determined from the slope of vertical stress-axial strain plot. After 1% of axial strain, when the viscous flow behavior governs material response, the initial shear modulus G_0 is calculated from the initial void ratio and mean stress (Hardin and Richart 1963). Since the initial stiffness increases with increasing strain rate (Matesic and Vucetic 2003), G_0 in the proposed model is given by

$$G_0 = C_g\left[(2.17 - e_0)^2\big/(1+e_0)\right]\sqrt{p'p_a}\left(1 + b_{rate}\ln\left(1+\dot{\varepsilon}_{eq}\right)\right) \tag{5}$$

where C_g is a model parameter, e_0 is the initial void ratio, p_a is a reference mean stress (= 100 kPa) and b_{rate} is a parameter that determines the dependence of G_0 on the applied deviatoric strain rate $\dot{\varepsilon}_{eq}$.

The shear modulus follows the Ramberg-Osgood type degradation given by Loukidis and Salgado (2009):

$$G = G_0\Big/1 + 2(1/\alpha_1 - 1)\left(\sqrt{3/2}\sqrt{r_{ij} - \alpha_{ini,ij}}\big/2\alpha_1 LI(G_0/p')\gamma_1\right) \tag{6}$$

where G is the degraded shear modulus, α_1 and γ_1 are model parameters and $\alpha_{ini,ij}$ is the initial value of the kinematic hardening tensor α_{ij}. The parameter LI represents the loading index: LI = 1 for loading, = 2 for subsequent unloading and reloading. The degradation of the shear modulus occurs both inside and outside of the yield surface and G is not allowed to degrade below $G_0/2(1/\alpha_1 - 1)$.

3.2 Incorporation of viscoplastic rate-dependence

The viscoplastic process begins as the stress-state reaches the yield surface. In this paper, Perzyna's overstress theory (Figure 2a) is used to incorporate the viscoplastic behavior of sand. The overstress theory is based on the viscoplastic overstress function ϕ defined as

$$\langle\phi(F)\rangle = \begin{cases} F \text{ if } F > 0 \\ 0 \text{ if } F \leq 0 \end{cases} \tag{7}$$

where the parameter quantifies the amount of overstress and is given by $F = f_d - f_s$ in which f_d and f_s are the dynamic and static yield surfaces, respectively.

Unlike the conventional, single yield-surface plasticity models, there is no static yield surface f_s in our model. In order to use the overstress theory, we assume that, at any given instance of time n, the yield surface f, given by equation (1), represents the static yield surface f_s and the "current" stress state, represented by r_n in Figure 2b, is on f_s. For the next strain increment at time n+1, if the stress state lies outside this static yield surface, then the stress state is viscoplastic. According to Liingaard et al. (2004), the "overstress" is the amount of stress by which a stress state exceeds the yield surface. Therefore, the stress state r_{n+1}^{visco} in Figure 2b, representing the stress state at time n+1, is on a dynamic yield surface f_d and the difference $\left| r_{n+1}^{visco} - r_n \right|$ represents the overstress. The dynamic yield surface is assumed to have the same form as equation (1). Thus, f_d is given by

$$f_d = \sqrt{\rho_{ij}^d \rho_{ij}^d} - \sqrt{2/3}m = 0 \tag{8}$$

where ρ_{ij}^d is the viscoplastic stress ratio, given by

$$\rho_{ij}^d = r_{ij}^d - \alpha_{ij} \tag{9}$$

In which r_{ij}^d is the measure of the current normalized deviatoric stress. Note that ρ_{ij}^d is the amount of "extra" stress from the centre α_{ij} of the yield surface (ρ_{ij}^d represents the distance of r_{n+1}^{visco} from the center of the yield surface in Figure 2b). Therefore, the measure of the overstress $\left| r_{n+1}^{visco} - r_n \right|$ can be obtained by appropriately subtracting the radius m of the yield surface from ρ_{ij}^d. The right hand side of equation (9) represents this "distance" $\left| r_{n+1}^{visco} - r_n \right|$ and hence f_d is the overstress in our model. Thus, we choose $F = f_d$ in our model.

Following Perzyna (1966), the total strain rate $\dot{\varepsilon}_{ij}$ is split into elastic and viscoplastic components $\dot{\varepsilon}_{ij}^e$ and $\dot{\varepsilon}_{ij}^{vp}$ as

$$\dot{\varepsilon}_{ij} = \dot{\varepsilon}_{ij}^e + \dot{\varepsilon}_{ij}^{vp} \tag{10}$$
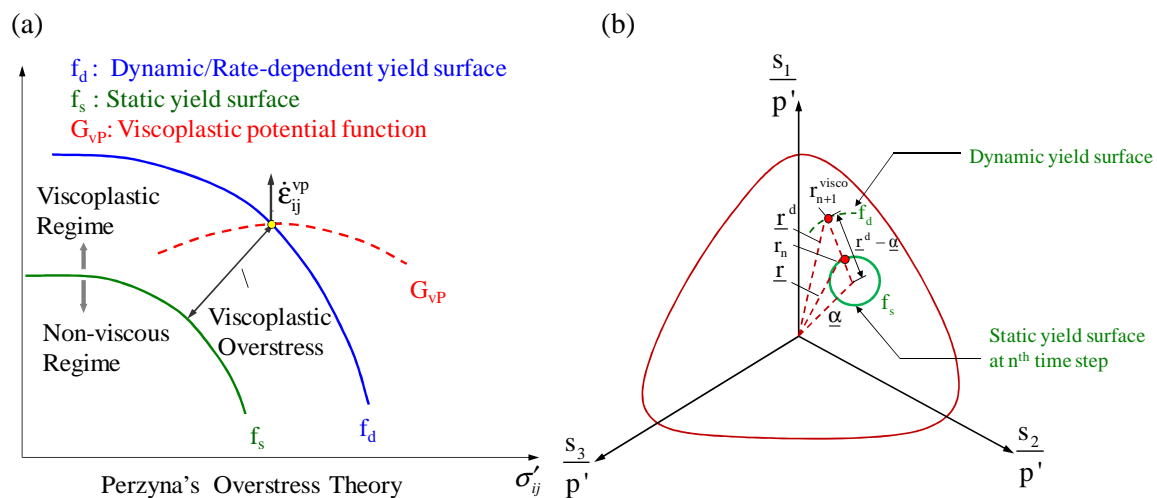
Figure 2. (a) The concept of overstress viscoplastic model (from Liingaard et al. 2004) and (b) initial ('static') and dynamic yield surfaces in the current model

The viscoplastic strain-rate ($\dot{\epsilon}_{ij}^{vp}$) is given by a non-associated flow rule

$$\dot{\epsilon}_{ij}^{vp} = \dot{\lambda}_{vp}\left(\partial G_{vP}/\partial\sigma_{ij}\right) \tag{11}$$

where G_{vP} is the viscoplastic potential function and $\dot{\lambda}_{vp}$ is the viscoplastic multiplier given by

$$\dot{\lambda}_{vp} = \langle\phi(F)\rangle/\eta \tag{12}$$

In which the parameter η is the viscoplastic coefficient. During the stress-strain integration, the viscoplastic multiplier is determined incrementally (Martindale et al. 2010). The gradient $\left(\partial G_{vP}/\partial\sigma_{ij}\right)$ of the viscoplastic potential in stress space is divided into a deviatoric component R'_{ij} and a mean component that relates to the dilatancy D (Loukidis and Salgado 2009):

$$\partial G_{vP}/\partial\sigma_{ij} = \left(R'_{ij} + 1/3 D\delta_{ij}\right) \tag{13}$$

R'_{ij} gives the direction of the deviatoric viscoplastic strain rate $\dot{e}_{ij}^{vp}$. The dilatancy D controls the shear-induced viscoplastic volumetric strain rate $\dot{\epsilon}_{kk}^{vp}$. D depends on the distance between the current stress state and the projected stress state on the dilatancy surface (Manzari and Dafalias 1997):

$$D = D_0/M_{cc}\left(\sqrt{2/3}\left(M_d - m\right) - \alpha_{ij}n_{ij}\right) \tag{14}$$

where D_0 is an input parameter controlling the inclination of the stress ratio-dilatancy curve.

4. MODEL PARAMETERS

We demonstrate the performance of the constitutive model by comparing the stress-strain responses obtained from our model with those obtained from SHPB tests performed by Felice (1985) on New Mexico clayey sand, Semblat et al. (1999) on Fontainebleau sand, and Veyera and Ross (1995) on Ottawa sand. Details of these sands are presented in Table 1.

The rate-indepedent parameters for Ottawa sand are available from Loukidis and Salgado (2009). Determination of the rate-independent model parameters for New Mexico clayey sand and Fontainebleau sand for modified Manzari-Dafalias model is underway. The current viscoplastic model formulation has two rate-dependent parameters η and b_{rate}. The coefficient of viscosity η of sand is assumed to be equal to 0.005 MPa-sec following Towhata (2008). The parameter b_{rate} is assumed to be equal to 0.002 for Ottawa sand and New Mexico clayey sand considering the fact that a 10% increase in the initial shear modulus value was observed for each log-cycle increase in the strain rate (Matesic and Vucetic 2003). For Fontainebleau sand, Semblat et al. (1999) observed a 0.2% decrease in the initial shear modulus value with each log-cycle increase in strain rate. Therefore, b_{rate} is assumed to be equal to −0.0001 for this sand. The rate-dependent model parameters for all the three sands are presented in Table 1.

Table 1: Description of sands used in model parameter determination

Sand	Type	Density (kg/m³)	Critical state friction angle (º)	Rate-dependent model parameters (from calibration)		References
				η (MPa-sec)	b_{rate}	
Ottawa sand	Silica sand	1715.00	29	0.005	0.002	Veyera and Ross (1995)
New Mexico clayey sand	Quartz sand	1870.00	$\approx$ 33 (considered to be the same as a Quartz sand)	0.005	0.002	Felice (1985) Lancelot (2006)
Fontainebleau sand	Quartz sand	1667.00	29	0.005	-0.0001	Semblat et al. (1999), Gaudin et al. (2005)

5. MODEL VALIDATIONS

5.1 Split Hopkinson Pressure Bar test

The developed constitutive model was incorporated in the finite element (FE) software Abaqus through a user material subroutine UMAT. SHPB tests were simulated at different strain rates for the New Mexico clayey sand, Fontainebleau sand and Ottawa sand using Abaqus. Table 2 presents the initial conditions of the SHPB simulations — sample dimension, density, initial void ratio and amplitude of loading — as used by Felice (1985) for New Mexico clayey sand, Veyera and Ross (1995) for Ottawa sand and Semblat et al. (1999) for Fontainebleau sand. The sand samples were assumed to be dry for the simulation. The tests were simulated using an axisymmetic 8-noded full integration element. Zero vertical-displacement and zero radial-displacement conditions were applied at the bottom and the side boundaries of the element, respectively, to simulate the uniaxial loading condition of the actual tests. Pressure loading (for New Mexico clayey sand and for Ottawa sand) or velocity boundary condition (for Fontainebleau sand) was applied on the top boundary of the specimen with exactly similar amplitudes as used in the actual experiments to simulate the uniaxial loading condition of the actual tests. Figure 4a illustrates the geometry of the sample for the New Mexico clayey sand. The analysis was performed in two steps: (1) geostatic equilibrium and (2) dynamic loading. Although there was no initial confining pressure applied in the actual tests, we applied a minimal initial confining stress of 20 kPa in the geostatic equilibrium stage to avoid numerical singularity. The dynamic loading step is simulated using the implicit dynamic procedure in Abaqus. Damping is applied in the dynamic loading step through material viscoplasticity.

Table 2: Description of initial test conditions and loading

Sand	Sample Dimension		Initial void ratio	Applied strain rates	Loading	Reference
	Height (cm)	Diameter (cm)				
Ottawa sand	0.635	5.08	0.545	1000/sec, 2000/sec	Applied pressure pulse, peak stress rise time 50 μsec, 257μsec pulse width	Veyera and Ross (1995)
New Mexico clayey sand	0.65	6.12	0.46	1051/sec	Applied pressure pulse, peak stress rise time 100 μsec, 140μsec pulse width	Felice (1985)
Fontainebl-eau sand	1.00	4.00	0.54 (same as e_{min})	393/sec, 771/sec, 1245/sec	Applied impact velocity, 3.4m/sec, 5.8m/sec, 9.9m/sec	Semblat et al. (1999), Vincens et al. (2003)

Figure 4b shows the vertical stress-time response of New Mexico clayey sand at 1051/sec strain rate. Figures 5a and 5b show the axial stress-strain response obtained from simulations of Fontainebleau sand and Ottawa sand respectively at different strain rates. The peak strengths of sands at high strain rate are predicted reasonably well. The model captures the initial high stiffness of the stress-strain curves for Ottawa sand and Fontainebleau sand through the initial increase in shear modulus. According to Veyera and Ross (1995), the initial steep slope of the stress-strain curves is caused by particle reorientation under high impact loading. The constitutive model in its present form does not capture sand behavior at the particle level. Further investigation is in progress to capture the particular behavior of sand at high loading rate and the gradual transition from the initial inertial response to the final exponential response of the curve.

(a)

(b)
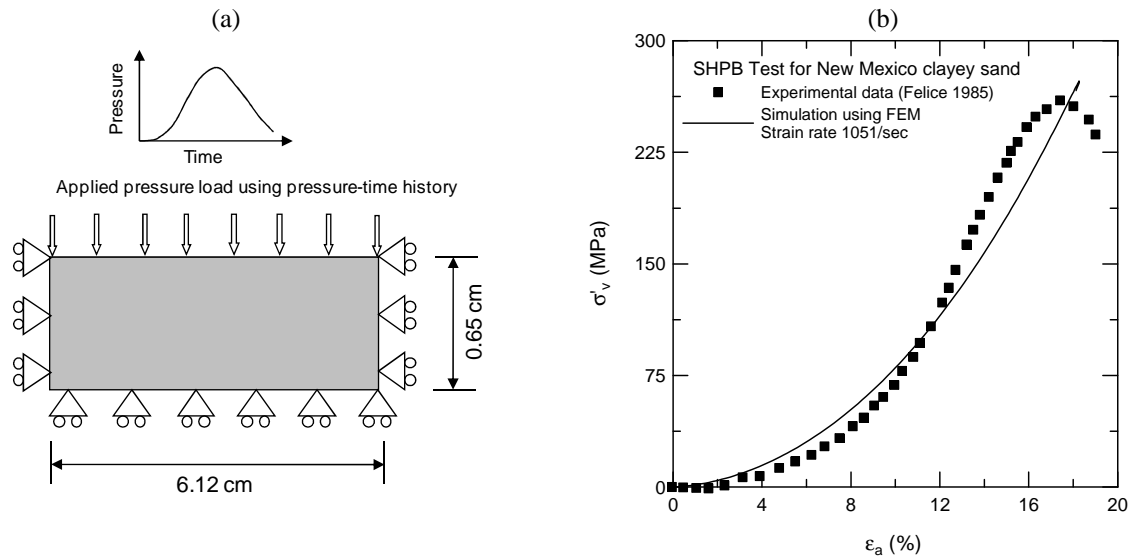
Figure 4. (a) Geometry of the SHPB test sample and (b) vertical stress-axial strain response of New Mexico clayey sand in SHPB test.

(a)

(b)
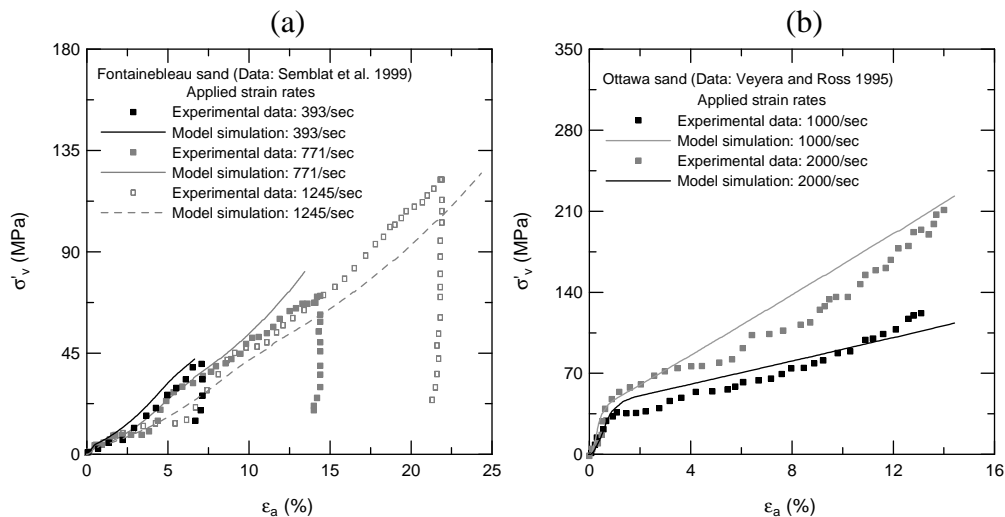
Figure 5. Vertical stress-axial strain response of (a) Fontainebleau sand and (b) Ottawa sand in SHPB test.

6. CONCLUSIONS

The paper presents a viscoplastic constitutive model for sand based on the concepts of critical-state soil mechanics for the design of sustainable civil infrastructure. The model is developed from an existing rate-independent sand constitutive model with open, "cone"-shaped yield and bounding surfaces. We added Perzyna's overstress function and the strain-rate dependence of the initial shear modulus to the existing rate-independent model in order to capture the viscoplastic, rate-dependent behavior of sand. The model is currently capable of simulating sand behavior up to a strain rate of 3000/sec. The peak strength of sand at high loading rates is captured reasonably well. Further investigation is in progress to capture the particular behavior of sand and the gradual transition from the initial inertial response to the final exponential response of the curve.

The incorporation of the rate-dependence was achieved by using two additional parameters that can be directly determined either through inspection of the experimental data or by fitting simple equations to laboratory test data. The model performance under high loading rate was demonstrated for Ottawa sand, New Mexico clayey sand and Fontainebleau sands. The paper outlined a part of an ongoing research on a systematic study of the mechanical response of soil subjected to extremely high strain rates.

References

Barsoum, R. G. S. and Philip, D. 2007. Armor including a strain rate hardening elastomer, *US Patent 7300893*.

Been, K. and Jefferies, M. G. 1985. A state parameter for sands. *Géotechnique*, 35 (2): 99-112.

Casagrande, A., and Shannon, W. L. 1948. Strength of soils under dynamic Loads. *Proceedings of the American Society of Civil Engineers*, 74(4): 591–608.

Chakraborty, T., Salgado, R. and Loukidis, D. 2010. A two-surface plasticity model for clay. *Submitted to Computers and Geotechnics*.

Dafalias, Y. F. and Manzari, M. T. 2004. Simple plasticity sand model accounting for fabric change effects. *Journal of Engineering Mechanics, ASCE*, 130: 622- 634.

DeSilva, C. W. 2005. Vibration and shock handbook. *Taylor and Francis, CRC Press*, 1872p.

Dupaix, R. B., and Boyce, M. C. 2007. Constitutive modeling of the finite strain behavior of amorphous polymers in and above the glass transition. *Mechanics of Materials*, 39:39–52.

Felice, C. W. 1985. The response of soil to impulse loads using the split-Hopkinson pressure bar technique. *PhD thesis*, The University of Utah, Utah, USA.

Gaudin, C., Schnaid, F. and Garnier, J. 2005. Sand characterization by combined centrifuge and laboratory tests. *International Journal of Physical Modelling in Geotechnics*, 1: 42-56.

Grujicic, M., Pandurangan, B, Cheeseman, B. A. 2006. A computational analysis of detonation of buried mines. *Multidiscipline Modeling in Materials and Structures,* 2: 363–387.

Hardin, B. O. and Richart, F. E., Jr. 1963. The nature of stress-strain behavior of soils. *Journal of Soil Mechanics and Foundations Division*, ASCE, 89 (1): 33-65.

Ishihara K. 1996. Soil behaviour in earthquake geotechnics. *Oxford Clarendon Press*, 259-260.

Jackson, J. G., Rohani, B., and Ehrgott, J. Q. 1980. Loading rate effects on compressibility of sand. *Journal of Geotechnical Engineering Division, ASCE*, 106(8): 839–852.

Kelln, C., Sharma, J. and Hughes, D. 2008. A finite element solution scheme for an elastic–viscoplastic soil model. *Computers and Geotechnics*. 35: 524–536.

Kumar, S., Chander, R. and Khattri, K.N. 1987. Compressional wave speed in the second crustal layer in Garhwal Himalaya. *Journal of Association of Exploration Geophysicists*, 8(4): 219-25.

Laine, P. and Sandvik. A. 2001. Derivation of mechanical properties for sand., *Proceedings of the 4th Asia–Pacific conference on Shock and Impact Loads on Structures*. Singapore 361–368.

Lancelot, L., Shahrour, I. and Mahmoud, M. A. 2006. Failure and dilatancy properties of sand at relatively low stresses. *Journal of Engineering Mechanics*, 132(12): 1396-1399.

Li, X. S. and Dafalias, Y. F. 2000. Dilatancy of cohesionless soils. *Géotechnique*, 50: 449-460.

Liingaard, M. Augustesen, A. and Lade, P. V. 2004. Characterization of models for time-dependent behavior of soils. *International Journal of Geomechanics*, 4(3): 157-177.

Loukidis, D. and Salgado, R. 2009. Modeling sand response using two-surface plasticity. *Computers and Geotechnics*, 36: 166–186.

Manzari, M. T. and Dafalias, Y. F. 1997. A critical state two-surface plasticity model for sands. *Géotechnique*, 47(2): 255-272.

Martindale, H., Higgins, W., Chakraborty, T., Basu, D. 2010. Two-surface viscoplastic sand model for high rate loading. Accepted in *International Conference on Geotechnical Engineering, ICGE Tunisia*.

Matešić, L. and Vucetic, M. 2003. Strain-rate effect on soil secant modulus at small cyclic strains. *Journal of Geotechnical and Geoenvironmental Engineering, ASCE*, 129 (6): 536–549.

Ortiz, M. and Simo, J. C. 1986. An analysis of a new class of integration algorithms for elastoplastic constitutive relations. *International Journal for Numerical Methods in Engineering*, 23: 353-366.

Perzyna, P. 1963. The constitutive equations for rate sensitive plastic materials. *Quarterly of Applied Mathematics,* 20: 321-332.

Perzyna, P. 1966. Fundamental problems in viscoplasticity. *Advances in Applied Mechanics*, 9: 244–377.

Semblat, J. F., Phong, L. M. and Gary, G. 1999. 3D-Hopkinson bar: new experiments for dynamic testing on soils. *Soils and foundation*, 39(1): 1-10.

Simo, J. C. and Hughes, T. J. R. 1998. Computational Inelasticity, *Springer*, 392p.

Sloan, S.W. 1987. Substepping schemes for the numerical integration of elastoplastic stress-strain relations. *International Journal for Numerical Methods in Engineering*, 24(5): 893-911

Song, B., Chen, W. and Luk, V. 2009. Impact compressive response of dry sand, *Mechanics of Materials*, 41: 777–785.

Tong, X. and Tuan, C. 2007. Viscoplastic cap model for soils under high strain rate loading. *Journal of Geotechnical and Geoenvironmental Engineering, ASCE*, 133(2): 206-214.

Towhata, I. 2008. Geotechnical Earthquake Engineering. *Springer.*

Tseng, T. and Chen, W. 2004. Contrasts in seismic wave speeds and density across the 660-km discontinuity beneath the Philippine and the Japan Seas. *Journal of Geophysical Research*, 109: B4, 12 pp.

Veyera, G. E. and Ross, C.A. 1995. High strain rate testing of unsaturated sands using a split-Hopkinson pressure bar, *Proceedings of 3rd International Conference on Recent Advances in Geotechnical Earthquake Engineering and Soil Dynamics*, St-Louis, USA, 31-34.

Vincens, E. Dubujet, Ph. and Cambou, B. 2003. Cyclic behavior of soils, a prediction of permanent deformations. *Deformation Characteristics of Geomaterials*, eds. Di Bendetto et al., Swets & Zeitlinger, Lisse: 1027-1034.

Wang, Z., Hao, H. and Lu, Y. 2004. A three-phase soil model for simulating stress wave propagation due to blast loading, *International Journal for Numerical and Analytical Methods in Geomechanics*, 28: 33–56.

Whitman, R. V. and Healy, K. A. 1962. Shear strength of sands during rapid loading, *Journal of the Soil Mechanics and Foundations Division*, *ASCE,* 88 SM2: 99-132.

Yamamuro, J. A. and Abrantes, A. E. 2003. Behavior of medium sand under very high strain rates. *Proceedings of 1st Japan-U. S. Workshop on Testing, Modeling, and Simulation*, Boston, MA, USA, 61-70.

Yamamuro, J. A. and Lade, P. V. 1998. Steady-state concepts and static liquefaction of silty sands. *Journal of Geotechnical and Geoenvironmental Engineering*, *ASCE*, 124(9): 868–877.